Journal of Visualization, Vol. 2, No. 2 (1999) 159-167

The Role of Visualization in Clarifying Interfacial Heat and Mass Transfer Mechanisms

De Angelis, V.* and Banerjee, S.*

* Department of Chemical Engineering, University of California Santa Barbara, Santa Barbara, CA 93106, USA.

Received 16 April 1999.
Revised 2 July 1999.

***Abstract*:** Mechanisms governing heat and mass transfer at air-water interfaces may be studied experimentally and by mean of Direct Numerical Simulations (DNS). Flow visualizations play a central role in unraveling the mechanisms that govern these transfer rates. In particular visualizations show that the flow is organized in large structures. These are sweeps, high-speed (relative to the interface velocity) fluid traveling toward the interface, and ejections, low speed fluid moving away from the interface region. It is the frequency with which these large flow structures refresh the interface that controls mass transfer.

On the liquid side, flow fluctuations in the near-interface region are relatively unimpeded, so fluid poor in solute can be transported by sweeps to the interface, and then pick up solute through diffusion before being carried away again. On the gas side, flow fluctuations in the near-interface region are strongly impeded, so mass transfer is controlled by sweeps and ejections, i. e., any events with significant interface-normal velocity.

The frequency, with which these large flow structures are generated, can be computed from the DNS. Simple parameterizations, based on the mechanisms discussed above, can be developed and appear to predict mass transfer velocities in excellent agreement with experimental and numerical results. The parameterizations capture the effect of capillary waves.

***Keywords*:** mass transfer, capillary waves, DNS, turbulent flow.

1. Introduction

Prediction of scalar transfer rates at the interface between non-mixable, turbulent streams is of central importance in environmental processes. Even though for short-time predictions, calculations of atmospheric conditions can be uncoupled from the general oceanic circulation calculations, still for longer-term climate predictions, interactions between the atmospheric and the oceanic circulation is critical. In fact, the oceans act something like flywheels, storing information about past climatic conditions that cumulatively impact their large-scale motions.

The rates at which exchanges occur at the interface affect quantities vital to climate, such as atmospheric concentrations of water vapor and greenhouse gases like CO_2. They also affect the oceanic circulation itself, which is largely driven by stresses at the surface imposed by the wind, i.e., by momentum exchange with the atmosphere.

Phenomena taking place over a wide range of length scales need to be considered. Momentum exchange is significantly affected by the form of the waves - "form" drag - and is controlled by the relatively large amplitude waves, with lengths of the order of meters. A portion of momentum exchange is associated with friction between air and water, and this "frictional" drag is affected by waves with length scales of the order of millimeters to centimeters. The controlling resistance to moisture transfer, in the absence of sprays, lies in layers with thickness of the order of millimeters. Exchanges of gas, like CO_2, are controlled by resistance in layers, now on the water side, that have thickness of the order of one hundredth of a millimeter.

It is clear that there is a multiplicity of scales involved in the exchange processes. At one end of the spectrum there is the need to model the general circulation of the atmosphere and oceans, and the nature of the global wave field, a task for meteorologists and oceanographers. At the other end of the spectrum there is the need to better understand the microphysics of transport processes dominated by fine-scale turbulence e.g. in gas exchange which is controlled by layers ≈ hundredth of a millimeter thick.

The scalar-transfer controlling phenomena are characterized by low Reynolds numbers when these are based on thickness of the layers containing the main resistance to transfer. Therefore direct numerical simulation

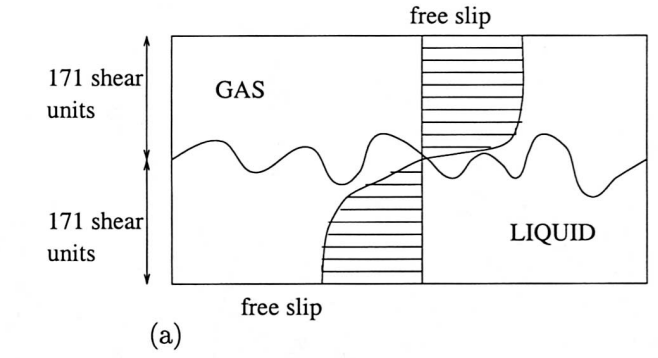

(a)

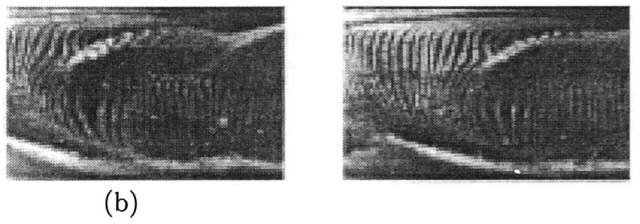

(b)

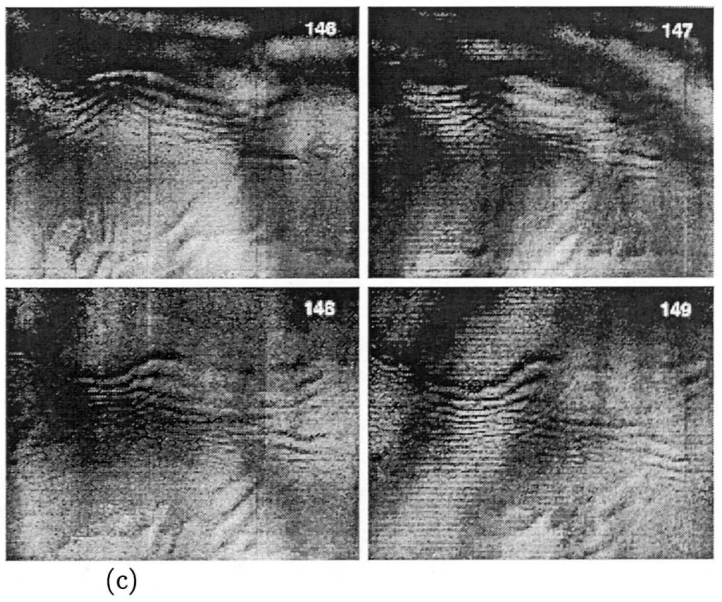

(c)

Fig. 1. (a) Domain geometry. The gas is on the top, liquid on the bottom. The two streams flow counter-currently; (b) Bursts in the liquid phase - side view. The gas-liquid interface is on the top, the wall is on the bottom. Gas (not shown in the figure) is flowing from L to R. Liquid is flowing from R to L. Bursts generate at the interface and at the wall, then are stretched in the direction of the flow ; (c) Four consecutive images of capillary waves. The wind speed is 5 m/s and wind is blowing from the top down. The time delay between images is 33 ms. the horizontal dimensions is 15 cm, the vertical dimension 19 cm. Taken from Kline and Jahne (1995).

(DNS) becomes possible. Such simulations produce a great deal of detailed information about the flow structure and the concentration field in the near interface region, and visualization becomes central in unraveling the various mechanisms. The typical flow geometry is shown in Fig. 1(a). Gas and liquid flow counter-currently and they interact at the interface, being coupled by boundary conditions requiring continuity of stress and velocity. Results in this manuscript apply to both heat and mass transfer with the assumption that the heat generated by friction is negligible and that the solute is dissolved in small amount.

2. Turbulence Structure, Waves and Mass Transfer: an Overview

Consider now experimental conditions set to keep the liquid Froude number and the gas velocity low enough to be well away from interfacial instabilities. A non-wavy surface can be obtained even when quite high shear rates are imposed, as shown by Rashidi and Banerjee (1990).

They visualize the liquid side flow, using a micro bubble tracer technique, in a situation in which there is a wall at the bottom of the liquid stream. The high-speed, low-speed streaks seen by many investigators are, of course, still found near the wall. However similar structures are also seen at high enough shear rates at the interface - whereas at low shear rate the interface structure looks patchy (S. Kumar et al ., 1998). Clearly there is a shear rate at which transition occurs, but once streaks are established in the near interface region, the similarity between the bursts seen in the vicinity of the wall and of the interface is remarkable. This is shown in Fig. 1(b), representing a side view of the liquid stream, with gas on the top going countercurrent to the liquid.

We now turn our attention to the characteristics of capillary waves. The wave spectrum on the air-water interface is rather complicated, and full numerical simulation is difficult. Here we concentrate on waves that form on the length scales of the coherent turbulence structures, as they can be important for mass transfer. These are relatively small ripples, usually are seen riding on the top of longer waves.

The photographs in Fig. 1(c) show these waves. They are taken from a manuscript of Klinke and Jahne (1995). The wind is blowing down from the top of the figures. The ripples appear to have wavelengths $\approx$ 1 cm. Regions with ripples alternate with regions in which the interface appears flat. Typical wave amplitude is less than 1 mm.

Values of mass transfer coefficient broadly increase with wind speed. Large scatter is seen due to the difficulty to measure concentrations in thin water layers near the air-ocean interface and due to the uncertainty on the actual value of the wind velocity. McCready and Hanratty (1985) attempted to explain mass transfer rates through flows driven by the shear stress fluctuations over the profile of waves. They found a peak frequency of the wave spectrum that closely corresponds to the value of the peak frequency of sweeps - large-scale motions impinging on the interface. Since sweeps and waves oscillate with almost the same frequency, it is not clear whether sweeps or wave-induced fluctuations are responsible for the increase of mass transfer observed on the liquid side of sheared interfaces.

Direct Numerical Simulations (DNS) can prove very useful in this case. The length scales of interest are accessible with present computational resources. The effect of turbulence on mass transfer across a flat interface can be studied, i.e. in the limit of low Weber and Froude number. Then the interface can be relaxed and capillary waves form. Thus the influence of the waves on the scalar fluxes can be determined.

3. Gas Liquid Flow across Flat Interface

We first conduct simulations in which we maintain the interface flat. This situation corresponds to the experiment of Rashidi and Banerjee (1990). The density ratio is ρ_l/ρ_g = 1000, typical of the air-water system.

Quantities are normalized by using "inner variables" based on the shear stress at the interface. We define a shear velocity as $u_\tau = (\tau_i/\rho)^{1/2}$, where τ_i is the shear at the interface. Shear units are defined as $h^+ = z\, Re_\tau$, where $Re_\tau = (u_\tau L)/\nu = 171$, L is the length of the gas and liquid domain in the interface normal direction and z is the spatial coordinate normalized by L (see Fig. 1(a)).

First consider some characteristics of the 3D-velocity flow on the gas and liquid sides. Streaks are seen on both sides of the interface. Streaks are also seen for wavy interfaces and the visualizations for this case are shown in Fig. 4(c). In the figure contours of the fluctuating component of the streamwise velocity (in the main flow direction) are shown. Red indicates high speed, blue low speed fluid. Streaks of high- and low-speed fluid alternate with a spacing of $\approx$ 100 shear units.

Quasi-streamwise vortices - vortices with axes primarily in the streamwise direction - form in the turbulent boundary layer. They can be traced by a scalar indicator, Ω, that traces regions of rotational flow i.e. regions in which $\nabla \boldsymbol{u}$ has complex eigenvalues (Hirschberg, 1992).

Strong vortices are contained in the first $\approx$ 100 shear-based units. The length of the quasi-streamwise vortices can be $\approx$ 400 shear-based units, as already observed in several numerical simulations of channel flow (e.g. Bernard et al., 1993).

A close view of quasi-streamwise vortices shows that many of them originate very close to the interface, say within 1-2 shear-based units from it. At any given instant about one fifth of these vortices are "coupled" across the interface. Vortices are then stretched in the flow direction as observed in Fig. 2(a). In Fig. 2(a) we show a close-up of velocity vectors and a isocontour of the vortex indicator, Ω. A sweep on the gas side seems to pair with an ejection on the liquid side. In both cases, large organized motions are observed. To use this information in modeling, some sort of "average" behavior of the turbulence structure has to be determined.

Contour plots of the total shear stress at the interface, overlapped with the top view of an Ω isosurface taken at the same instant, are presented in Fig. 2(b) for the gas and for the liquid sides. In Fig. 2(b) (Top) the gas is flowing from left to right; the liquid flows from right to the left in Fig. 2(b) (Bottom). Contours of the total interfacial shear stress have a characteristic streaky distribution with a few patches of high shear stress. The origin of the vortices, when traced back to the interface in these two-dimensional top views, is usually located in areas of transition between high and low shear stress. The shear stress distribution is continuous at the interface, however, because the gas is observed from the top and the liquid from the bottom the shear stress contours in the top and bottom figures appear to be the mirror image of each other.

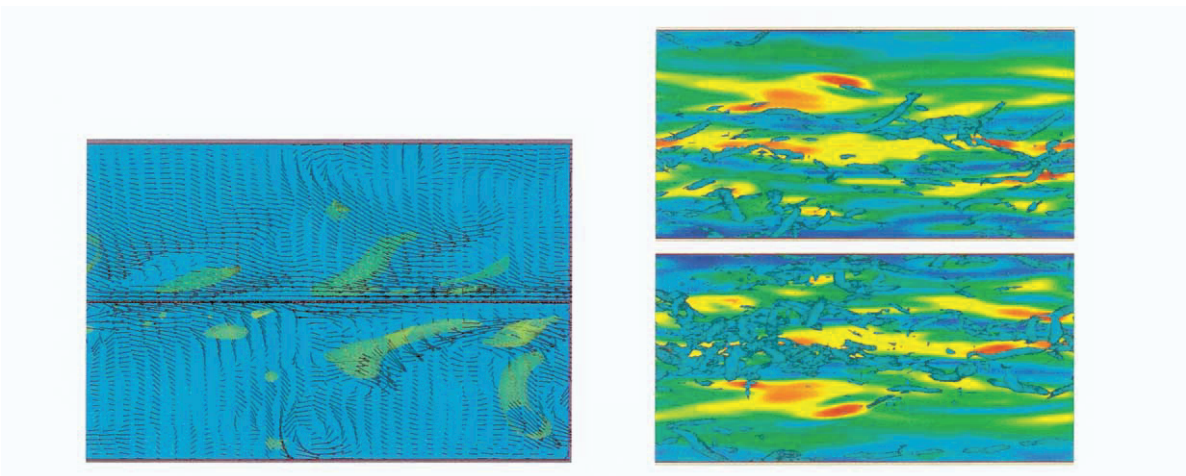

(a) (b)

Fig. 2. (a) Sweep-ejection pair in the near-interface region. The figure shows a cross-section in the plane defined by the mean-flow direction and by the interface-vertical direction. The interface is in the middle of the figure. Gas is on the top flowing from L to R. Liquid is on the bottom flowing from R to L; (b) Shear stress on the interface and quasi-streamwise vortices. Gas is on the top flowing from L to R. Liquid in on the bottom flowing from R to L. The intense blue corresponds to $\tau = 0.30\ Re_\tau$ and the intense red to $\tau = 1.5\ Re_\tau$.

At this point it is worth considering how the high shear stress regions form. This can be clarified by considering a quadrant analysis of the velocity field over the interface in which velocity fluctuations in each quadrant of the Reynolds stresses are correlated with shear stress at the interface. Refer to the cartoon in Fig. 3. Consider the velocity flow in a plane parallel to the interface. Then when the streamwise velocity fluctuations are positive (I and IV Quadrant) the flow is traveling faster than the mean average velocity on the plane, and when the interface normal velocity is positive (I and II Quadrant) the flow is directed from the boundary toward the center of the domain. In the first quadrant both the streamwise and interface normal velocity fluctuations are positive. In the second, the streamwise component is negative but the interface normal component is positive. This corresponds to an ejection of low speed fluid. In the third quadrant both the streamwise and the interface-normal velocity fluctuations are negative, and in the fourth the streamwise component is positive whereas the interface-normal component is negative. The fourth quadrant then corresponds to a sweep in which high-speed fluid is brought

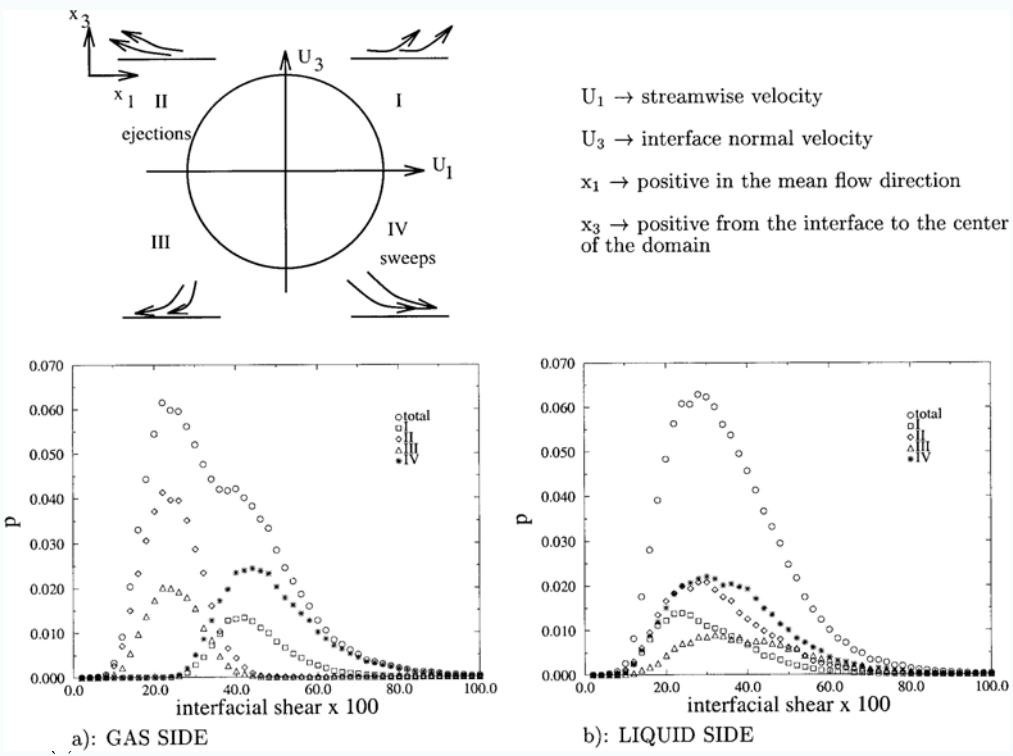

Fig. 3. Top: Definition of quantities used for Reynolds stresses quadrant analysis. Bottom: Probability of strongly coherent events according to Reynolds stress quadrant as a function of interfacial shear stress in the region over which the events occur. (a) gas; (b) liquid.

towards the interface. Consider now the correlation of each quadrant of such velocity fluctuations with the interfacial shear stress shown in Fig. 3(a) on the gas side. It is clear that sweeps, i.e., in the fourth quadrant, lead to the high shear stress regions whereas ejections lead to the low shear stress regions. This is what is observed in wall turbulence at a solid boundary and therefore the gas sees the liquid surface much like a solid boundary. However, if we look at Fig. 3(b), it is immediately clear that no such correlation exists on the liquid side. In fact, all the quadrants have similar behavior with regard to the shear stress regions.

The difference between the gas and the liquid phases in the near interface region is further clarified by observing the velocity fluctuations on each side of the interface (Lombardi et al., 1996). The gas behaves much like flow over a solid wall. The fluctuations are almost identical to that at a solid boundary, in all directions - streamwise, spanwise, and wall-normal. On the other hand, the liquid has the largest fluctuations in the streamwise and spanwise directions right at the interface itself. It sees the interface virtually as a free slip boundary, except for the mean shear..

4. Gas-liquid Flow across Deforming Interface

When the interface is free to deform two new parameters enter the analysis: the Froude number (Fr) and the Weber number (We), these are defined as $We = (\rho h u\tau^2)/\gamma$ and $Fr = (u\tau^2\rho)/(gh\,(\rho_l - \rho_g))$.

The numerical method cannot handle wave breaking so We and Fr have to be chosen carefully. This limits the shear velocity to $\approx$ 0.3 m/s on the gas side. This implies, for an air-sea system, a 10 m wind velocity of $\approx$ 7.5 m/s, or a 5 m wind velocity of $\approx$ 5 m/s. In this case (case D1) a steady wave spectrum in the capillary region can be obtained. For larger values of the wind velocity, waves grow quickly and the calculations have to stop. We will show some flow snapshots for a 10-meter wind velocity of 11 m/sec (case D2).

The wave amplitudes in cases D1 are $\approx$ O (1 mm) and the wave spectrum has a peak for a wave number of $\approx$3.5 cm^{-1}. This is in agreement with the observation of Komori et al. (1993) who report amplitudes of $\approx$ 1mm for comparable wind speeds. The computational domain dimensions are roughly 12 cm in the streamwise direction, 6

cm in the spanwise direction and 2 cm in the interface-normal direction. This covers a range of wave numbers, in the flow direction, of 1 cm^{-1} to 15 cm^{-1} that coincides with the wave number range of the waves in Fig. 1(c).

We analyze in detail the three-dimensional structure of the velocity, shear and pressure field for case D2. A snapshot of the interface shape is shown in Fig. 4(a). The wave altitude has been amplified five times its actual value. The contours indicate shear stress levels. The red regions are high shear stress regions. The blue regions correspond to low shear stress. The gas is on the top flowing from right to the left. The liquid is on the bottom, flowing in the opposite direction. The high shear stress regions correspond to the wave crests. In the concave regions the shear is low. Occasionally circulation on the gas side can be observed. This can be seen in the close-up of Fig. 4(b). The streamlines are in a plane defined by the vertical to the interface and by the mean-flow direction. The gas moves first over a wave crest and then circulates in the valley. The liquid has much higher inertia and the streamlines stay attached to the boundary. Pressure - not shown here - is discontinuous on the two sides of the interface, as required by the normal stress boundary condition. On the gas side pressure is lower on the wave crests and high in the wave valleys. On the liquid side the opposite trend is observed.

Even if the form of the waves dominates the patterns of shear stress and pressure, streaks are still seen to form on the two sides of the interface. In Fig. 4(c) we show the contour of the streamwise velocity fluctuations on the gas side (at $z^+ = 10$) and on the liquid side (at $z^+ = 8$). Streaks are seen in both domains. The streak length is not organized on the wave patterns, and the spacing in between streaks is also $z^+ = 100$ - as for wall- and flat-interface turbulence.

Results of quadrant analysis, done following the same methodology used for the flat-interface case, confirms the differences between gas and liquid sides. Sweeps and Quadrant I events are more probable on the gas side for high shear stress values and ejections and Quadrant III events are more probable for low values of the shear stress. On the liquid side there is no such a separation.

The frequency spectrum of the wave amplitude is obtained over a time interval of $T^+ = 350$ for case D1. This is reported in De Angelis (1998). It shows a peak for $T^+ = 22$ that corresponds closely to the frequency peak measured by McCready and Hanratty (1985). Also the peak value is in good agreement. Time spectra of Reynolds stress show instead a peak for $T^+ \approx 50$. This value is in good agreement with the sweep and ejection frequency measured by Rashidi and Banerjee (1990)

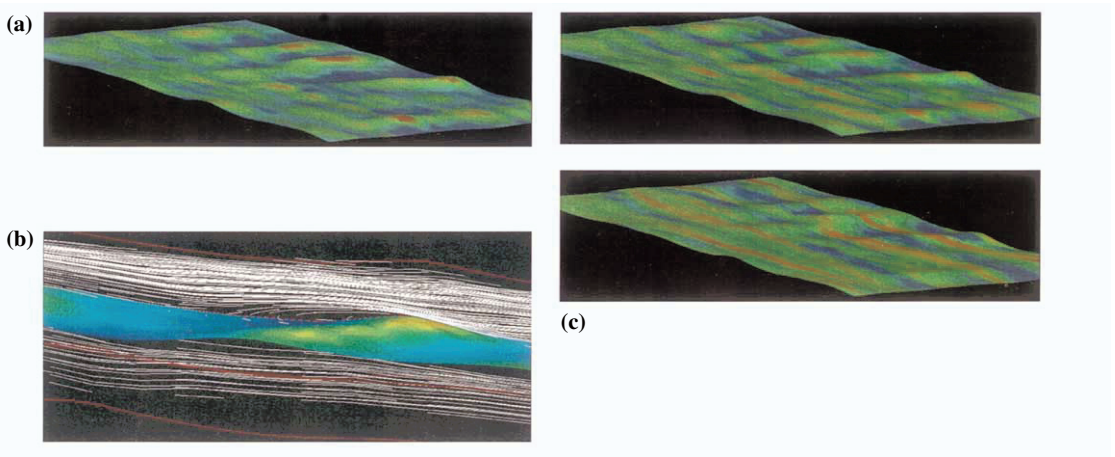

Fig. 4. (a) Wave profile at the interface. The red is high shear, blue is low shear. The gas is on the top flowing from R to L. The liquid is on the bottom, flowing from L to R. The shear is high in the peaks and low on the walleyes of the wave profile; (b) Close up of the flow in the near-interface region. The gas flow shows circulation in the walleyes of the wave profile. The liquid stays attached at the interface because of its higher inertia. The gas flows from R to L. The liquid from L to R; (c) Contours of the fluctuating part of the streamwise velocity. The top plane is for the gas side with flow from R to L. The bottom plane is for the liquid side with flow from L to R.

5. Scalar Transfer Behavior

Mass transfer velocity can be normalized using u_τ. A non-dimensional velocity can be defined as $\beta^+ = 1/(2^{1/2} Re_\tau Sc (c_o - c_b)) du/dx_3$, where du/dx_3 is the non-dimensional gradient at the interface and c_b and c_o are the bulk andinterface concentrations. The values of β^+ on the gas and liquid sides are shown in Fig. 5. The value of β^+

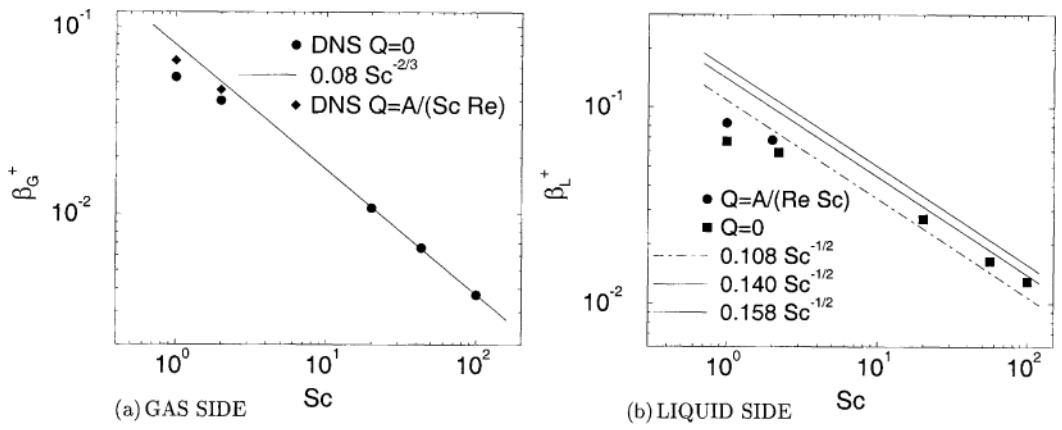

Fig. 5. Mass transfer velocity on the gas, (a), and liquid, (b), sides for different values of the Schmidt number. Also the parameterizations developed in the next section are shown. Points for Sc = 1 and Sc = 2 are computed also by using a source term in the scalar-advection equation (see De Angelis, 1998 for details).

scales as $Sc^{-2/3}$ on the gas side and $Sc^{-1/2}$ on the liquid side.

We extended the quadrant analysis of Fig. 3 and look at the correlation of the Reynolds stress - and therefore of the turbulence structure, in the various quadrants with the instantaneous value of mass transfer velocity β^+ at the interface. Results are reported in De Angelis (1998) and summarized here. On the liquid side sweeps correlate with the highest values of β^+ at the interface for both Schmidt number 1 (low) and 100 (high). On the gas side, for Sc =1, I and IV quadrant events correlate well with high β^+, but for Sc =100, sweeps and ejections play the dominant role.

When waves form on the interface, we do not observe significant changes in the value of β^+ on the gas and liquid sides. Changes are of O(5–10%) which is within the statistical error. Having said this, we do observe a slight trend. The value of β^+ on the liquid side is seen to increase with wave amplitude. On the gas side the values decrease.

6. Modeling

We will attempt, now, modeling of mass fluxes based on surface renewal concepts. Surface renewal theory hypothesizes that the mass flux across an interface is governed by renewals of the interfacial fluid by motion of the bulk fluid. Scalar transfer proceeds by unsteady diffusion into renewed regions of the surface till the fluid is replenished and the process starts again. Of course the issue is to determine the frequency of such renewals.

In Fig. 6(a) we show a comparison between the DNS results and the prediction of surface renewal theory on the liquid side for Sc = 56. In the bottom of the figure the Reynolds stress and the vertical fluctuating velocity are shown as time proceeds. When they are both negative, a sweep is impacting the interface. In the center figure the corresponding mass transfer velocity is shown and compared to the values predicted by surface renewal theory. The top figure shows the total mass flux over time. The dotted curve in the center and top figures are computed using, respectively $(D/(\pi t))^{1/2}$ and $2((D t)/\pi)^{1/2}$. They represent the instantaneous flux and the total flux, i.e., the time integral of the instantaneous flux, for transient diffusion into a stagnant media.

It appears that the mass transfer velocity increases when a sweep is present on the interface. The decay of the mass transfer velocity appears to be faster than $t^{-1/2}$. It should be noticed, however, that the sweep effect persists at the interface and travels with the liquid mean velocity, therefore its effect propagates further along the interface, leaving the point of observation. This means that, in a Lagrangian frame, the DNS is closer to the surface renewal theory.

To clarify this point, in Fig. 6(b) we report the contour of the Reynolds stress (bottom) and of the mass transfer velocity (top). The vertical axis is time, and the horizontal axis is the abscissa along a line parallel to the mean-flow direction. The graph describes how a sweep moves along a line parallel to the streamwise direction, as time passes. The arrows indicate a sweep event and the corresponding mass transfer velocity. The sweeps appear to survive for more than 300 wall units, and the high mass-flux patch moves with it.

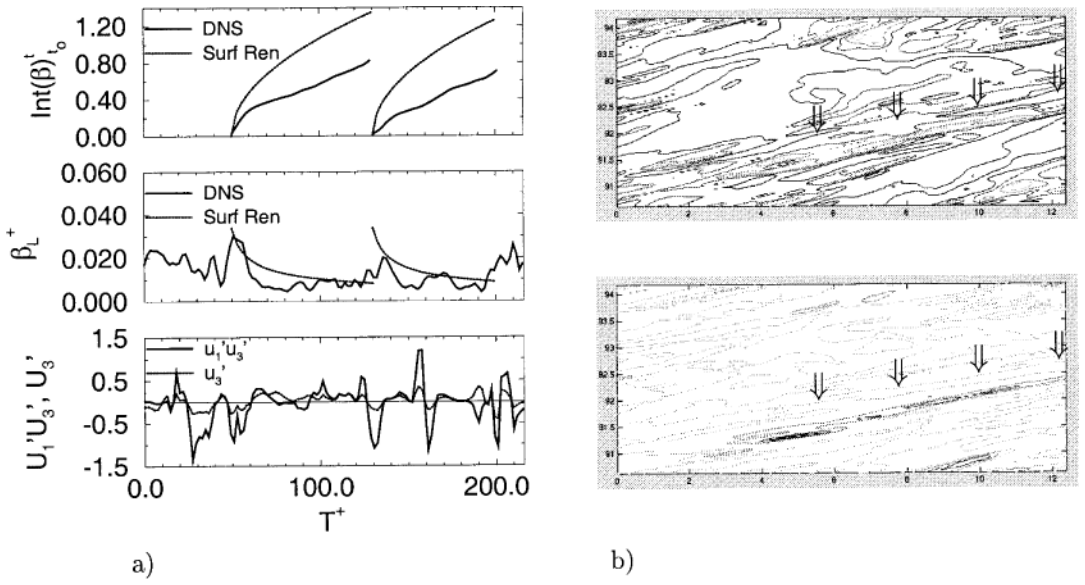

Fig. 6. (a) DNS and surface renewal theory; (b) Reynolds stresses (bottom) and β^+ (top) moving at different locations in the mean-flow direction (horizontal axis), as time passes (vertical axis). Quantities are normalized using quantities based on the shear at the interface u_τ for velocity, u_τ^2 for Reynolds stresses and $t^+ = \nu/u_\tau^2$ for time).

On the gas side, at first glance, it seems that surface-renewal modeling would be less appropriate. In fact we observed that large vertical (interface-normal) velocity fluctuations correlate with high mass-transfer rates. Large vertical fluctuations are, however, mainly related to the bursting process thus also supporting parameterizations based on surface renewal-type models with both sweeps and ejections being important.

Consider first the liquid side. In this case we use a parameterization proposed by Banerjee (1990). Consider the simple surface renewal expression, $\beta^+ = (D/T)^{1/2}$, and assume that $T = 30$ to 90 (ν/u_τ^2), where T is the time ranging between sweeps and bursts frequency. We then obtain the relation, $\beta^+ Sc^{1/2} = (0.108 \text{ to } 0.158)\ u_\tau$. This expression is compared with simulation results over a large range of Sc number [Fig. 5(b)]. Good agreement is found for the high *Sc* number cases. Values for the small *Sc* number cases lie well below the correlation. In fact, for Sc ≈ 1, diffusion is not negligible and transport is not through renewal events. Similar behavior at low Sc number is also observed in laminar boundary layer (Leal, 1992). From our DNS we obtain a value of $T^+ = 50$. This gives a coefficient of 0.14, that is also reported in Fig. 5(b). This expression has also been compared with wind-wave tank data for SF_6 transfer rates from Wanninkhof and Blivens (1991) in De Angelis (1998). Good agreement is found for wind speed comparable to that of the simulation. In this situation, in fact, the contribution of the form drag to the total drag is small.

Turning now to the gas side, the gas sees the liquid much like a solid surface as discussed earlier. So a form of the surface renewal theory modified for such applications, e.g. by Banerjee (1971) amongst others, is necessary. This leads to a different dependence in the Schmidt number, and the modified expression is of the form, $\beta^+ Sc^{2/3} = (0.07 \text{ to } 0.09)\ u_\tau$. Figure 5(a) compares the expression with DNS results. It is clear that the Schmidt number dependency is correctly predicted, and the numerical values are within the range of the expression. The lower bound of the expression compares well with the moisture transfer data of Ocampo-Torres et al. (1994) as reported in De Angelis (1998).

On the gas and liquid sides the value of β^+ changes slightly with wave amplitude. Reynolds stress and mass-transfer velocity increases on the liquid side and decrease on the gas side only slightly (De Angelis, 1998). Therefore the parameterizations still capture the main transfer mechanisms when capillary waves form. Of course the effect of u_τ cannot be fully investigated by DNS, given the limitation on the domain deformation that our numerical scheme can handle.

7. Conclusion

We started this manuscript by analyzing the length scales over which mass and heat transfer take place at a wavy interface. Because phenomena occur in layers of less that 1 cm, Direct Numerical Simulation can be used to calculate the quantities of interest. The simulations are restricted to a wave spectrum in the range of capillary

waves. The simulations showed that the turbulence structure on the gas and liquid side is similar to what observed in channel flow. These findings support the flow visualizations of Rashidi and Banerjee (1990).

The turbulence structure was also analyzed by mean of statistical tools. A quadrant analysis of the Reynolds stresses shows that the dynamics at the interface is governed by the gas side turbulence that sets the shear patterns at the interface. On the liquid side, fluctuations on the interface proceed almost unimpeded, because of the large inertia of the liquid. Therefore the flow structure can penetrate the near-interface region more on the liquid than on the gas side.

DNS supported the modeling of mass transfer in many ways. Results of the calculations gave values of the mass transfer velocity difficult to measure, and for cases with and without waves. Then visualization of turbulence structure and of mass transfer distribution over the interface suggested different mechanisms controlling mass transfer on the gas and liquid side. Statistical tools allowed determining the controlling events to be used in models based on renewal theory. Finally the parameters in the models could be computed directly from DNS results.

DNS should not be regarded only as a tool to obtain accurate statistics of various moments of the velocity field to then be used in turbulence closure models like LES or RANS. It is also as a photograph of phenomena that can guide modeling and suggest new avenues in the understanding of the formidable problem of turbulence and related transport phenomena.

References

S. Banerjee, "A note on Turbulent Mass Transfer at High Schmidt Numbers," Chem. Eng. Science, (1971), 26, 989-990.

S. Banerjee, "Turbulence structure and transport mechanisms at interfaces," Proceedings of the Ninth International Heat Transfe r Conference, Jerusalem, Israel, 1990, 395-417.

P. S. Bernard, J. M. Thomas and R. A. Handler, "Vortex dynamics and the production of Reynolds stress," J. Fluid Mech., 253, (1993), 385.

V. De Angelis, "Numerical Investigation and Modeling of Mass Transfer Processes at Sheared Gas-Liquid Interfaces," Ph.D. Disser tation, University of California at Santa Barbara, 1998.

G. S. Hirschberg, "Direkte Simulation der turbulenten Taylor-Couette Stromung und der ebenen Kanalstromung,",Ph.D. Dissertation , ETH-Zurich, (1992).

J. Klinke and B. Jahne, "Measurements of Short Ocean Waves during the MBL ARI WEST Coast Experiments," Air-water Gas Transfer - Third Int. Symposium on Air-Water Gas Transfer, (1995), 165-173.

S. Kumar, R. Gupta and S. Banerjee, "An experimental investigation of the characteristics of free-surface turbulence in channel flow," Physics of Fluids 10, (1998), 437.

L. G. Leal, "Laminar flow and convective transport processes: Scaling principles and asymptotic analysis," Butterworth-Heineman n, Stoneham (MA), USA, (1992).

P. Lombardi, V. De Angelis and S. Banerjee, "Direct numerical simulation of near-interface turbulence in coupled gas-liquid flo w," Physics of Fluid, 8, (1996), 1643-1665.

M. J. McCready and T. Hanratty, "Effect of air shear on gas absorption by a liquid film," AIChE Journal, 31(12), (1985), 2066-74.

F. J. Ocampo-Torres, F. J. Donelan, J.M. Woollen and J. R. Koh, "Laboratory measurements of Mass Transfer of Carbon Dioxide and water Vapor for Smooth and Rough flow conditions," Tellus Series B, 46, (1994), 16-28.

M. Rashidi and S. Banerjee, "The effect of boundary Conditions and Shear rates on Streaks formation and breakdown in Turbulent channel flow," Physics of Fluid, (1990), A2, 1827-38.

R. H. Wanninkhof and L. F. Bliven, "Relationship between gas exchange, wind speed, and radar back-scatter in a large wind wave tank," J. of Geophysical Research, 96(C2), (1991), 2785-2796

Authors' Profiles

Valerio De Angelis: He completed the Ph.D. program of the department of Chemical Engineering at UCSB in '98. He developed methods for DNS of turbulent flow and mass transfer at high Schmidt numbers. He is currently working in a software engineering company (MetaHeuristics-Santa Barbara (CA) 93105, US) where he is participating in the implementation of level-set methods (for multiphase flows) in commercial codes. His other scientific interests include artificial intelligence and gas-lattice methods. He can be contacted at valerio@anemone.ucsb.edu.

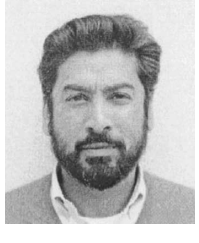

Sanjoy Banerjee: He has been active in investigating multiphase phenomena since the early '70s including the use of optical methods and DNS. His other academic interests include dynamic large-eddy simulation models, DNS methods based on wavelets, level-set methods for multiphase flows, flow visualization of wave micro breaking and development of new DPIV techniques. He can be contacted at banerjee@anemone.ucsb.edu.